III-4

Surface,
Interface and
Thin Films

BL2A

Zn L_3-edge XANES of ZnO Powder

E. Kobayashi[1], S. Yoshioka[2] and K. K.Okudaira[3]

[1]*Kyushu Synchrotron Light Research Center, Tosu 841-0005, Japan*
[2]*Gradiate School of Engineering, Kyushu University, Fukuoka 819-0395 Japan*
[3]*Graduate School of Science and Engineering, Chiba University, Chiba 263-8522, Japan*

Zinc oxide (ZnO) is an important material in devise [1] because of its wide band gap 3.37 eV and has a relatively large exciton binding energy of 60 meV. In recent years, organic photovoltaic (OPV) has been attracting attention as a low-cost, lightweight battery that replaces conventional solar cells. ZnO plays an play an essential role as an electron transporting layer (ETL) material. In order to further improve the characteristics of ETL, it is necessary to understand the electronic states. Near-edge X-ray absorption fine structure (NEXAFS) spectroscopy is a powerful tool for investigating the electronic structures of materials.

In this report, we investigated the electronic structure of ZnO powder by means of XANES using fluorescence yield method.

Zn L_3-edge XANES measurements were performed at the BL2A beamline of UVSOR Okazaki, Japan, using the partial fluorescence yield method (PFY). A Beryl double crystal monochromator defined Zn L absorption edges in the energy region from 1000 to 1090 eV. Fluorescence X-rays were collected using an energy dispersible silicon drift detector (SDD). All measurements of XANES spectra were carried out at room temperature.

Figure 1 shows the Zn L-edge NEXAFS spectra of ZnO powder and ZnO/Si film obtained from TEY.

The peak A provides information both about the forbidden electron transitions, which does not obey dipole selection rules and disorder in the crystal geometry [2]. The peak B and C are related to the transition of 2p core electrons to the Zn4p levels [2].

The spectral future marked as A in Zn L-edge NEXAFS spectra of ZnO powder is almost the same as that of ZnO / Si film, while the peaks B and C in Zn L-edge NEXAFS of ZnO powder are difference from those of ZnO / Si film. This suggests that the surface state of ZnO powder is different from that of ZnO / Si film since TEY is sensitive to the surface electronic states.

Figure 2 shows the Zn L-edge NEXAFS spectra of ZnO powder obtained from PFY. PFY (Zn L) is almost the same as the result of TEY, but PFY (O K) is different. This suggests that the surface and bulk of ZnO particles may have different electronic states of oxygen.

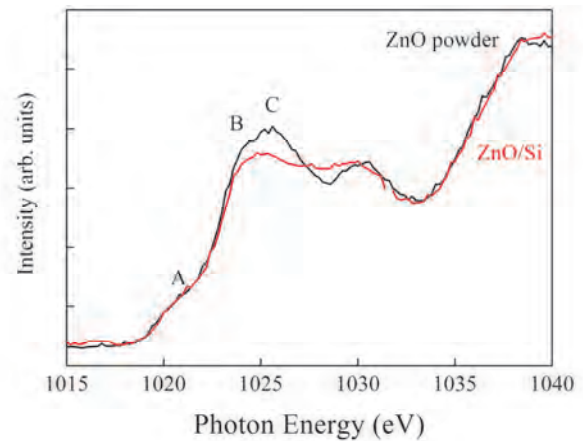Next, we will clarify how this electronic state changes when an organic layer is placed on ZnO.

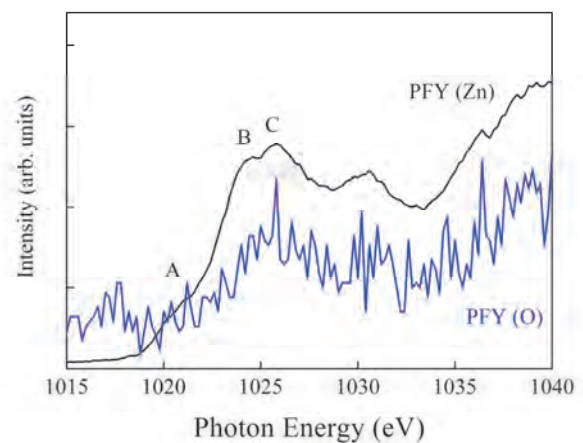Fig. 1. Zn L-edge XANES spectra of ZnO obtained from TEY. ZnO powder (black) and ZnO/Si film (red) spectrum.

Fig. 2. ZnO L-edge XANES spectra of ZnO powder obtained from PFY. PFY (Zn L) (black) and PFY (O Kα) (blue) spectrum of ZnO.

[1] F. Quaranta, A. Valentini, F. R. Rizzi, and G. Gasamassima, J. Appl. Phys. **74** (1993) 224.
[2] O. M. Ozkendir, S. Yildirimcan, A. Yuzer, K. Ocakoglu, Progress in NaturalScience:Materials International **26** (2016) 347.

BL2B

Electronic Structure of ZnO Nanoparticles as an Electron Extraction Layer for Organic Solar Cells

K. K. Okudaira and T. Kikuchi

Association of Graduate Schools of Science and Technology, Chiba Univererity, Chiba 263-8522, Japan

Organic devices such as organic photovoltaic cells have been attracting interest concerning both fundamental research and practical application for low-cost, large-area, lightweight and flexible devices. Conjugated polymer solar cells are attractive as a source of renewable energy due to the low cost by using roll-to-roll-printing processes. The most polymer solar cells have bulk heterojunction (BHJ) morphology. At this morphology, one of materials consisting of BHJ contacts directly the undesired electrode. To fabricate inverted polymer solar cells, one widely used approach is to deposit a thin film of zinc oxide (ZnO) nanoparticles as an electron extraction layer and a hole-broking layer on top of a transparent indium tin oxide coated substrate [2].

For nanoparticles, the contribution of surface to their electronic and optical properties is expected to be significant, because of their large surface area-to-volume ratio.

In this work we deposited ZnO nanoparticles (NPs) using spin-casting method on indium tin oxide (ITO) substrate and estimated the electronic structure of ZnO NPs by ultraviolet photoelectron spectroscopy (UPS) measurements with different exciting energies due to the photoionization cross-section.

UPS measurements were performed at the beam line BL2B of the UVSOR storage ring at the Institute for Molecular Science at the photon energy (hν) of 28 eV and 40 eV. ZnO NPs with uniform shape and highly dispersed were synthesized using zinc acetate dihydrate $(Zn(CH_3COO)_2·2H_2O)$ and potassium hydroxide (KOH) as a precursor and absolute ethanol as solvent via solvothermal method [3]. The thin films of ZnO NPs were deposited on ITO by spin casting (as-grown ZnO NP). The films were annealed at 140 °C in the atmosphere for 10 minutes (annealed ZnO NPs). The mean size of synthesized ZnO NPs was about 7 nm using TEM measurements.

We observed UPS of as-grown ZnO NPs and annealed ZnO NPs at hν of 28 eV and 40 eV (Fig. 1). The peak at binding energy (Eb) of about 10 eV at hν of 40 eV appears more clearly than that at hν of 28 eV. The calculated photoionization cross-section of Zn 3d at hν of 40.8 eV is much larger than that at hν of 26.8 eV, while that of O 2p at hν of 40.8 eV is smaller than that of 26.8 eV [4]. The peak at Eb of about 10 eV can be assigned to Zn-3d. The broad feature at Eb about 7 eV and 4 ~ 5 eV are attributed to mainly Zn-4s electrons and O-2p electrons, respectively [5]. The UPS structure at Eb about 5 eV changes by annealing. The O-2p states would be affected by annealing, due to disappearance of oxygen vacancies and/or formation of hydroxyl

groups at the surface of nanoparticles. Furthermore, the work-function of as-grown ZnO NPs can be estimated to 3.92 eV, which is lower than that of ITO (about 4.6 eV). This value is closer to the electron affinity of PCBM (3.82 eV) [6], which is a typical electron accepter material in BHJ. It is expected that the ZnO NP is good electron extraction layer for polymer solar cells.
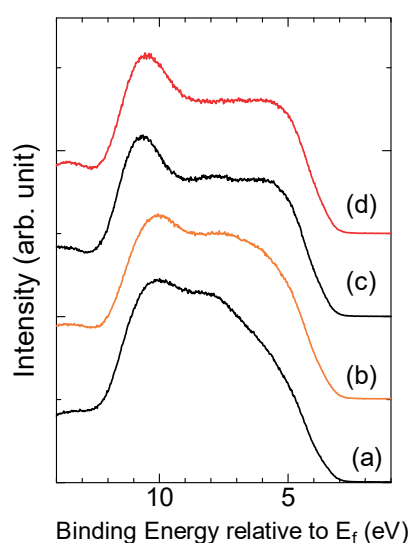

Fig. 1. UPS of (a) as-grown ZnO NPs at hν = 28 eV, (b) annealed ZnO NPs at hν = 28 eV (c) as-grown Zn NPs at hν = 40 eV, (d) annealed ZnO NPs at hν = 40 eV.

[1] X. Gu *et al*. Adv. Energy Mater. **7** (2017) 1602742.
[2] S. Kim *et al*. Chem. Commun. **49** (2013) 6033.
[3] N. M. Shamhari *et al*. Acta Chim. Slov. **65** (2018) 578.
[4] Atomic Calculation of Photoionization Cross-Sections and Asymmetry Parameters, J. -J. YEH, 1993, AT & T.
[5] W. Ranke, Solid state commun. **19** (1976) 685.
[6] H. Yoshida, J .Phys, Chem, C, **118** (2014) 24377.

BL3U

Layered Manganese Oxide Electrocatalyst Containing K⁺ Cation for Water Oxidation Studied by Operando XAFS Observations

S. Tsunekawa[1], M. Nagasaka[2], H. Yuzawa[2] and M. Yoshida[1]

[1]*Yamaguchi University, Tokiwadai, Ube 755-8611, Japan*
[2]*Institute for Molecular Science, Okazaki 444-8585, Japan*

Energy consumption is increasing in proportion to the world's population. This large energy consumption is leading to serious problems such as depletion of fossil fuels and increase in carbon dioxide emissions. In recent years, hydrogen production has been attracting attention as a CO_2-free energy source that does not rely on fossil fuels, and a hydrogen production process by water electrolysis using renewable energy sources has been proposed. However, the insufficient efficiency of oxygen evolution reaction (OER) restricts the efficiency of overall water splitting. In this situation, a potassium-including manganese oxide ($K:MnO_x$) was developed by Nocera group [1], and they reported that $K:MnO_x$ could decompose water to oxygen gas efficiently. Thus, we have investigated the structure and function of the $K:MnO_x$ catalysts during water splitting by operando soft, tender, and hard X-ray XAFS measurements.

The electrochemical cell was used with a Pt counter and an Ag/AgCl reference electrode. The $K:MnO_x$ catalyst was prepared by electrodeposition on Au thin film in a solution containing $MnCl_2$ and K⁺ cation. Under electrochemical control, the operando Mn K-edge and K K-edge XAFS were measured by fluorescence mode in the PF BL-9A, and the operando O K-edge XAFS was measured by transmission mode at BL3U in the UVSOR Synchrotron.

First, we checked the OER activity and found that $K:MnO_x$ function as highly efficient water splitting catalyst. The surface morphology and chemical composition were investigated by SEM, EDX and XPS. The Faraday efficiency for catalyst was estimated as about 100 % for production of oxygen and hydrogen gasses by quadrupole mass spectrometry.

Next, operando O K-edge XAFS was measured under electrochemical control, and the peak top position and shape of the spectra for the $K:MnO_x$ suggested that the electronic state of Mn species in the catalyst was similar with δ-MnO_2 (Fig. 1.). Then, operando Mn K-edge XAFS measurements showed that most of the Mn species were oxidized from Mn^{3+} to Mn^{4+} at 1.0V, although small amount of Mn^{3+} remained. Furthermore, the curve fitting of the Fourier transform of k^3 weighted EXAFS oscillation exhibited that the local structure of Mn species in the catalyst composed of δ-MnO_2 structure, which was similar to the conclusion of the operando O K-edge XAFS. On the other hand, operando K K-edge XAFS measurements showed that the hydrated K⁺ intercalated between the δ-MnO_2 layers. It is reported that the water splitting reaction proceeds at a Mn^{3+} sites in the δ-MnO_2 structure [2-4]. Thus, we

also suggest that the Mn^{3+} in the δ-MnO_2 layers function as the active sites for OER process [5].

In conclusion, we investigated the electronic state and local structure of $K:MnO_x$ electrocatalyst by operando O K-edge, Mn K-edge and K K-edge XAFS measurements. The result elucidates that the catalyst composed of δ-MnO_2 with layered structures containing hydrated alkali metal ion, and suggested that the water splitting reaction efficiently proceeded at the active sites of Mn^{3+}.
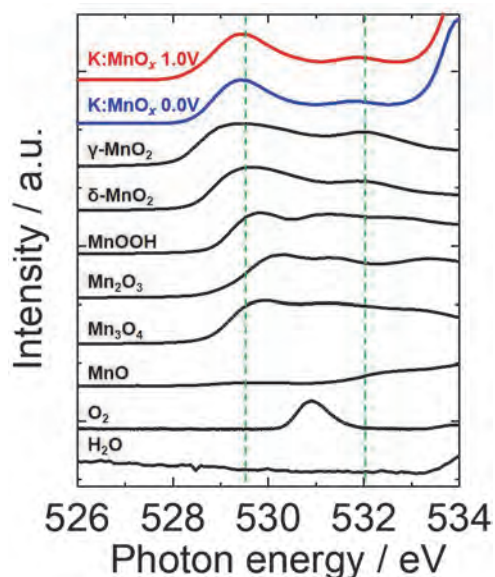

Fig. 1. Operando O K-edge XAFS spectra for $K:MnO_x$ and references.

[1] M. Huynh, D. Bediako and D. Nocera, J. Am. Chem. Soc. **136** (2014) 6002.
[2] T. Takashima, K. Hashimoto and R. Nakamura, J. Am. Chem. Soc. **134** (2012) 1519.
[3] M. Huynh, C. Shi, S. Billinge and D. Nocera, J. Am. Chem. Soc. **137** (2015) 14887.
[4] Y. Gorlin, B. Kaiser, J. Benck, S. Gul, S.Webb, V. Yachandra, J. Yano and T. Jaramillo, J. Am. Chem. Soc. **135** (2013) 8525.
[5] S. Tsunekawa, F. Yamamoto, K. Wang, M. Nagasaka, H. Yuzawa, S. Takakusagi, H. Kondoh, K. Asakura, T. Kawai and M. Yoshida, J. Phys. Chem. C. **124** (2020) 23611.

Ⅲ-4

BL3B

Control of Growth Orientation and Evaluation of Film Quality of UV Emitting Zinc Aluminate Phosphor Thin Films

H. Kominami[1], M. Endo[2], T. Kawashima[2], N. Sonoda[2], A. Fujii[1], K. Inoue[1],
N. Uesugi[1], K. Nie[1], A. Dorokhina[3] and S. Kurosawa[4,5]

[1]*Graduate School of Integrated Science and Technology, Shizuoka University, Hamamatsu 432-8651, Japan*
[2]*Faculty of Engineering, Shizuoka University, Hamamatsu 432-8651, Japan*
[3]*Graduate School of Science and Technology, Shizuoka University, Hamamatsu 432-8651, Japan*
[4]*New Industry Creation Hatchery Center (NICHe), Tohoku University, Sendai 980-8579, Japan*
[5]*Faculty of science, Yamagata University, Yamagata 990-8560, Japan*

The global pandemic of COVID-19 has led to frequent disinfection of hands and everywhere they can touch, and the pharmaceutical industry is rapidly developing vaccines. A "new normal" has been advocated, and it has become necessary not only to wear face masks and secure social distance, but also lifestyle habits including dietary habits that improve immune function are emphasized, and how to protect ourselves from viruses is important. It has become a re-concern in people's lives.

The UV light is used for various applications depending on the wavelength as well as the sterilization described above. The lights of 200-280nm (UV-C) region as for the sterilization, 280-320nm (UV-B) region as the treatment of the skin disease, 320-400nm (UV-A) region as application of purification of water and air, and photocatalysts. Recently, from the viewpoint of consideration to the environment, the mercury free UV emission devices have been demanded for the application of catalyst and medical situations. In our previous work, it was clarified that $ZnAl_2O_4$ phosphor was suitable for the UV field emission lamp because of its stability and luminescent property. It shows strong UV emission peaked around 250 nm which suitable for sterilization.

In this research, $ZnAl_2O_4$ layer were prepared by thermal diffusion of ZnO and sapphire substrate for new UV devices. To obtain $ZnAl_2O_4$ thin film with high quality, we explore optimum condition of thermal annealing, such as annealing temperature, atmosphere, and annealing time. From the experiment, optimum annealing conditions were obtained 990 ºC for 50 hours.

Figure 1 shows PLE spectra of $ZnAl_2O_4$ thin films prepared on 2 types of sapphire substrate, one-side polished and both-side polished. PL intensity of one-side polished substrate was higher than the both-side polished. It is thought that the possibility of total internal reflection occurs inside the board of the substrate. Therefore, it is necessary to determine the film thickness by fully considering the light extraction efficiency.

Figure 2 shows transmittance spectra of $ZnAl_2O_4$ thin film, compared with sapphire substrate. Excitation edges were observed around 180 nm and 380 nm. The edge of 180 nm was caused from $ZnAl_2O_4$, it consistent with the transmittance results. However, the edge of 380

nm was caused from slightly residual ZnO phase. In order to suppress the residual zinc oxide, it is necessary to carefully examine the film thickness of ZnO.
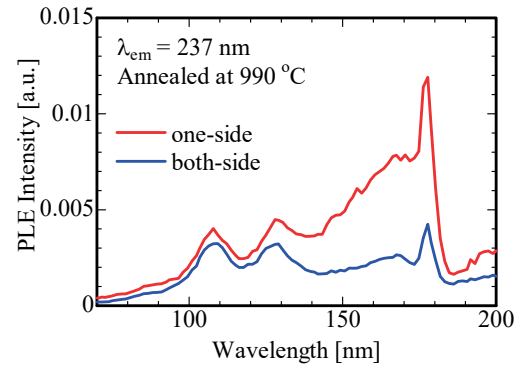

Fig. 1. PLE spectra of $ZnAl_2O_4$ thin films prepared on sapphire substrate of one-side polished and both-side polished.
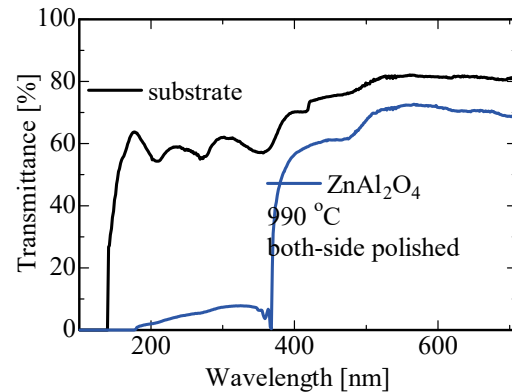

Fig. 2. Transmittance spectra of $ZnAl_2O_4$ thin film.

BL4B

Characterization of Amorphous Arsenic, Selenium and Arsenic Triselenide by Vacuum Ultraviolet Transmission Spectroscopy

K. Hayashi

Department of Electrical, Electronic and Computer Engineering, Gifu University, Gifu 501-1193, Japan

Amorphous chalcogenide semiconductor materials are very expected as a potential material for optoelectronic devices. Because, in these materials are very sensitive to the light, and show a variety of photoinduced phenomena [1-3]. Although many studies have been done on the photoinduced phenomena of these materials, little is known about the details of these mechanisms. These phenomena were studied by exciting outer core electrons with the irradiation of light with the energy corresponding to the optical bandgap or sub-bandgap. The interest has been attracted for the change of the optical properties in the energy region of the visible light. We are interesting for the changes of the optical properties in the higher energy region. To obtain a wide knowledge of the photoinduced phenomena, it is necessary to investigate to the photoinduced and annealing effects on wide energy region. In this report, we report the VUV transmission spectra of amorphous compound semiconductors and their constituent elements.

Samples used for the measurement of the VUV transmission spectra were amorphous arsenic, selenium and arsenic triselenide thin films prepared onto thin aluminum films by conventional evaporation technique. The sample thicknesses ranged between 100 and 200 nm. The aluminum film of the thickness of 200 nm was used to eliminate the higher order light from the monochromator in the VUV region. These measurements were carried out at room temperature at the BL4B beam line of the UVSOR facility of the Institute for Molecular Science. The spectrum was measured by using the silicon photodiode as a detector. Two pinholes of 1.5 mm in a diameter were inserted between the monochromator and sample to remove stray light. The intensity of the VUV light was monitored by measuring the TPEY of a gold mesh. The positions of the core levels for the samples were calibrated by referencing to the 2p core level absorption peak of the aluminum film.

Figure 1 shows the VUV transmission spectra of amorphous arsenic (a-As), selenium (a-Se) and arsenic triselenide (a-As$_2$Se$_3$) thin films. Two main absorption peaks were observed in this wavelength region for amorphous As$_2$Se$_3$. One absorption peak around 22nm corresponds to the 3d core level of Se atom. Another absorption peak around 28 nm corresponds to the 3d core level of As atom. As shown in the figure, each spectrum is very broad and multiple shoulders are observed. The absorption spectrum observed in the amorphous As$_2$Se$_3$ is roughly consistent with the previous report [4]. On the other hand, VUV

transmission spectra of amorphous As and Se are different from the previous report. Although the wavelength resolutions in the spectral measurements are all the same, the spin-orbit splitting of the 3d$_{5/2}$ and 3d$_{3/2}$ level of each atom is clearly resolved in amorphous As$_2$Se$_3$, while in amorphous As and Se are not clearly resolved. It is not clear about the origin of broad spectra and shoulders. I think that these origins are related to the local structures of the amorphous network. Therefore, it seems that it depends on the preparation method and the presence or absence of annealing. The detailed experiments and analysis will be done in the next step. More detailed experiments are necessary to clarify the origin of the VUV transmission spectra.
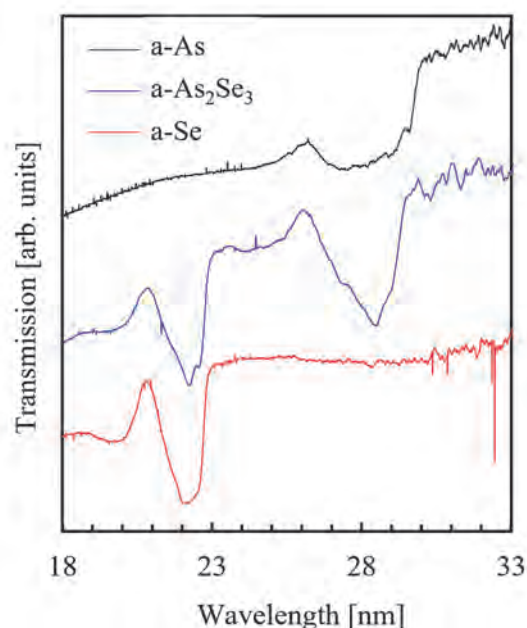
Fig. 1. VUV transmission spectra of a-As, a-Se, and a-As$_2$Se$_3$ thin films.

[1] K. Tanaka, Rev. Solid State Sci. **4** (1990) 641.
[2] K. Shimakawa, A. Kolobov and S. R. Elliott, Adv. Phys. **44** (1995) 475.
[3] K. Tanaka, Encyclopedia of Nanoscience and Nanotechnology **7** (2004) 629.
[4] J. Bordas and J. B. West, Phil. Mag. **34** (1976) 501.

BL4B

Structural and Magnetic Properties of FeCo Alloy Multilayer Thin Films Grown by Nitrogen Surfactant Epitaxy on Cu(001)

T. Miyamachi[1], K. Yamamoto[2,3], T. Koitaya[2,3] and T. Yokoyama[2,3]
[1]The University of Electro-Communications, Chofu 182-8585, Japan
[2]Institute for Molecular Science, Okazaki 444-8585, Japan
[3]The Graduate University for Advanced Studies, SOKENDAI, Okazaki 444-8585, Japan

Ⅲ-4

An $L1_0$-type FeCo ordered alloy attracts much attention as a rare-earth free magnetic material due to its large magnetic anisotropy, large magnetic moment, and high Curie temperature. Intensive works has been carried out to fabricate $L1_0$-FeCo phase with uniaxial anisotropy. Using pulsed laser deposition, the growth of FeCo thin films with alternating Fe and Co atomic layers was investigated [1]. However, the $L1_0$ structure is a non-equilibrium state of FeCo phase and hence its fabrication method has not been established yet. The main problem could be caused by the atomic-scale disorder at the Fe/Co interface during growth processes, which suggests the importance of microscopic characterizations of structural, electronic and magnetic properties of $L1_0$-FeCo.

To improve the quality of FeCo alloy thin films, we intend to incorporate nitrogen surfactant effects of monatomic layer magnetic nitrides into the alternate atomic-layer Fe and Co deposition. In this method, the nitrogen surfactant epitaxy of monatomic layer magnetic nitride with high lateral lattice stability can suppress the interdiffusion at the Fe/Co interface during the deposition and annealing processes, which results in atomically flat surface/interface. The important role of the nitrogen surfactant effect on the fabrication of high quality $L1_0$-type alloy thin films has been demonstrated for FeNi alloy thin films [2].

In this study, we here performed combined study of scanning tunneling microscopy (STM) and x-ray absorption spectroscopy/x-ray magnetic circular dichroism (XAS/XMCD) to investigate structural, electronic and magnetic properties of FeCo alloy multilayer thin films by the nitrogen surfactant epitaxy. This complementary experimental approach enables to link macroscopic observations of element specific and quantitative electronic and magnetic properties by XAS/XMCD with microscopic origins of the Fe/Co interface characteristics revealed by STM [3]. FeCo alloy multilayer thin films was grown on Cu(001) in the following processes: (1) the monatomic layer iron nitride (Fe_2N) was firt grown on Cu(001) [4], (2) 1 ML Co was deposited at a low temperature (~ 150 K) and annealed at room temperature, (3) alternating layer deposition of Fe and Co was repeated to fabricate multilayers.

XAS/XMCD measurements were performed at BL4B in UVSOR by total electron yield mode at B = 0 - ± 5 T and T = 7.3 K. The XMCD spectra are obtained at the normal (NI: $\theta = 0°$) and the grazing (GI: $\theta = 55°$) geometries by detecting $\mu_+ - \mu_-$, where μ_+ (μ_-) denotes the XAS recorded at Fe and Co L adsorption edges with the photon helicity parallel (antiparallel) to the sample magnetization. Note that θ is the angle between the sample normal and the incident x-ray. Magnetization curves were recorded by plotting the L_3 XAS intensity normalized by the L_2 one as a function of the magnetic field.

We first confirmed from XMCD measurements the strong in-plane magnetic anisotropy of bare Fe_2N as previously reported [4]. STM measurements revealed that adding Co 1 ML on Fe_2N results in the formation of $Co_2N/Fe/Cu$ (001) via nitrogen surfactant effect. Accordingly, relative increase in the out-of-plane magnetization of Fe to the in-plane magnetization was observed. We found from thickness dependence of Fe magnetization curves that the out-of-plane magnetization of Fe was further increased by repeating alternative depositions of Fe and Co. The results possibly reflect the intrinsic out-of-plane magnetization of $L1_0$ FeCo and indicate that the nitrogen surfactant effect efficiently suppress the interdiffusion at the Fe/Co interface and keep atomically flat surface/interface in FeCo atomic layers.

[1] H. Ito *et al*., AIP Advances **9** (2019) 045307.
[2] K. Kawaguchi *et al*., Phys. Rev. Materials, **4** (2020) 054403.
[3] S. Nakashima *et al*., Adv. Funct. Mater. **29** (2019) 1804594.
[4] Y. Takahashi *et al*., Phys. Rev. B **95** (2017) 224417.

BL4B

Ground State and Magnetic Properties of Iron Phthalocyanine Thin Films Grown on a Monolayer Graphene Sheet

S. Ohno[1], I. Sakaida[1], K. Yamamoto[2,3], T. Koitaya[2,3] and T. Yokoyama[2,3]

[1]College of Engineering Science, Yokohama National University, Yokohama 240-8501, Japan
[2]Institute for Molecular Science, Okazaki 444-8585, Japan
[3]The Graduate University for Advanced Studies, SOKENDAI, Okazaki 444-8585, Japan

Iron phthalocyanine (FePc) is one of the prototype molecules to study magnetic properties of molecular thin films. It is a planner molecule which has an Fe^{2+} iron at the center. The ground state of an FePc molecule has been a controversial issue. Density functional theory (DFT) calculations showed that the calculated density of states (DOS) at the valence band region agree well with the experimental data [1]. However, it was found to be quite difficult to determine the ground state symmetry unambiguously because of the similarity of the calculated DOS even for the ground states with different symmetries. X-ray absorption spectroscopy study suggested that the ^3E_g ground state with the half-filled e_g state at the Fermi level is plausible for FePc thin films grown on gold surfaces [2]. In the present work, we focused on the ground state and magnetic properties of FePc thin films grown on a monolayer graphene sheet, which is produced by chemical vapor deposition (CVD) and transported onto the silicon oxide substrate (Gr/SiO$_2$).

BL4B soft X-ray beamline was used for X-ray Absorption Near Edge Structure (XANES) spectroscopy measurements in N K-edge and Fe L-edge regions, and X-ray Magnetic Circular Dichroism (XMCD) measurements in Fe L-edge region.

We have reported on our previous results for FePc thin films grown on passivated silicon surfaces as well as a graphene sheet [3]. Here, we report on our new results on the high-resolution XANES spectra, and some further analysis on the magnetic properties.

Figures 1 (a) and (b) show XANES spectra taken at the incident angle of Θ = 0º and 65º, respectively. These results agree well with the previous assignment of the spectral components based on the ^3E_g ground state [2].

Tilt angle of the molecular plane of FePc can be evaluated based on the conventional analysis method[4]. The obtained value is ~24º in the present case. The applicability of the full analysis using the sum rules is based on the assumption that the FePc molecule takes the adsorption configuration of the flat-lying orientation and has D$_{4h}$ symmetry in the point group representation [2]. Present XANES spectra shown in Fig. 1 is quite similar to those in the other reports[2,5], suggesting that the sum rules can be applied approximately.

Thus, we could have obtained a series of physical quantities related to the magnetic properties of FePc. For example, the ratio of the orbital moment in the molecular plane (m_L^{xy}) and the spin moment (m_s) is evaluated to be ~1.0, even larger than the reported value of ~0.8 [2]. This indicates that the enhancement of the orbital moment is promoted by the contact with the graphene sheet.
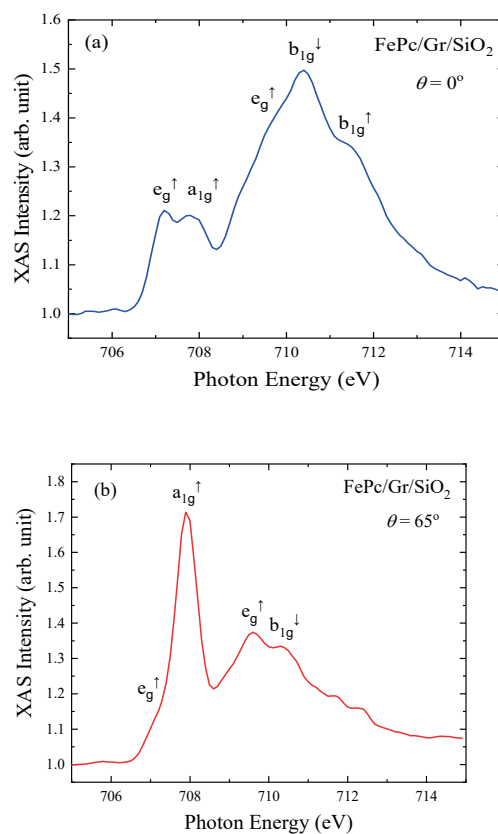

Fig. 1. Angle-dependent linearly polarized XANES spectra for FePc/Gr/SiO$_2$.

[1] N. Marom *et al.*, Appl. Phys. A **95** (2009) 165.
[2] J. Bartolomé *et al.*, Phys. Rev. B **81** (2010) 195405.
[3] S. Ohno *et al.*, UVSOR Activity Report 2019 **47** (2020) 133.
[4] J. Stöhr, "NEXAFS Spectroscopy" (Springer).
[5] S. Lisi *et al.*, J. Phys. Chem. Lett. **6** (2015) 1690.

113

BL5U

Observation of Electronic Band Structure in Two-dimensional WSe₂ Flake

M. Sakano[1], Y. Tanaka[1], S. Masubuchi[2], S. Okazaki[3], K. Watanabe[4], T. Taniguchi[5],
T. Sasagawa[3], T. Machida[2] and K. Ishizaka[1]

[1]*Quantum-Phase Electronics Center and Department of Applied Physics, The University of Tokyo, Tokyo 113-8656, Japan*
[2]*Institute of Industrial Science, The University of Tokyo, Tokyo 153-8505, Japan*
[3]*Materials and Structures Laboratory, Tokyo Institute of Technology, Yokohama 226-8503, Japan*
[4]*Research Center for Functional Materials, National Institute for Materials Science, Tsukuba 305-0044, Japan*
[5]*International Center for Materials Nanoarchitectonics, National Institute for Materials Science, Tsukuba 305-0044, Japan*

Development of fabrication techniques for exfoliated two-dimensional (2D) flakes enables us to investigate the physical properties of the 2D materials. In 2D materials, peculiar physical phenomena that do not appear in bulk crystals are realized because the electronic band dispersion discretely changes as the layers decrease to the monolayer limit. However, due to the limited size of the flake samples (typically ~10 μm), it is a challenging task to precisely determine the electronic structures of various two-dimensional materials.

In our study, we have developed a procedure to fabricate flake samples that can be adapted to various 2D materials and investigated the electronic band dispersions of monolayer WSe₂ by performing micro-focused angle-resolved photoelectron spectroscopy (micro-ARPES).

The samples were fabricated by an all-dry pick-up and flip method (see ref. [1] for details). As shown in Fig. 1 (a), the monolayer WSe₂ is encapsulated with graphene to prevent oxidation of the WSe₂, and electrically contacts to an Au electrode fabricated on a SiO₂/Si substrate though graphite to prevent charging up. The fabricated sample is pumped and sealed in an ICF-70 nipple with a gate valve, and transported to the ultrahigh vacuum chamber. Before the micro-ARPES measurement, the sample is annealed around 200 °C for ~10 hours in the ultrahigh vacuum.

Figure 1 (b) shows an obtained ARPES image. Unfortunately, although we could observe the photoelectron intensities of the graphene and/or graphite, but not observe those of the monolayer WSe₂. After the measurement, the spot size of the synchrotron light was evaluated and found to be much larger than the size of the WSe₂ flake (~20 μm) in the setup at that time. For future measurements, it is necessary to make the spot size of the synchrotron light comparable to the size of the fabricated sample before performing the ARPES measurement.
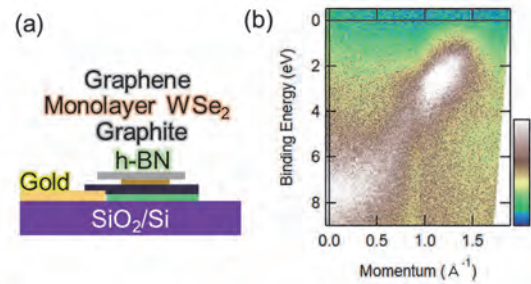

Fig. 1. (a) A schematic of a fabricated monolayer WSe₂ flake (typical size ~20 μm) sample for micro-ARPES measurement. The monolayer WSe₂ electrically connects to an Au electrode fabricated on a SiO₂/Si substrate through graphite. To prevent oxidation of the WSe₂ flake, the topmost is covered by graphene (typical size ~100 μm). The detailed fabrication process is written in ref. [1]. (b) Obtained ARPES image. The photoelectron intensities from the graphite and/or graphene can be observed, but not clearly from the monolayer WSe₂.

[1] M. Sakano *et al.*, arXiv:2103.11885 (2021).

BL5U

Electronic Structures of Transition Metal Phosphide (TMP) Thin Films on TMP Substrates

N. Maejima[1,2], T. Yoshida[1], Y. Shimato[1] and K. Edamoto[1,2]

[1] Coll. Sci., Rikkyo Univ., Tokyo 171-8501, Japan

[2]Research Center for Smart Molecules, Rikkyo Univ.,Tokyio 171-8501, Japan

Transition metal phosphides (TMPs) have attracted much attention because of their high catalytic activities for hydrodesulfurization (HDS). Among TMPs studied thus far, Ni_2P shows the highest catalytic activity while that of Fe_2P is extremely low [1]. Recently it has been found that, when some of Ni atoms in Ni_2P are substituted by Fe atoms (denoted as NiFeP, hereafter), the reaction path is changed from a hydrogenation path to a direct desulfurization path [2]. Such a change in selectivity should be closely related to the change in the electronic structure of active Ni sites due to the charge transfer between Ni, Fe and P atoms. In this study, we investigate the electronic structures of Ni_xP/Fe_2P and Fe_xP/Ni_2P, which can be viewed as model systems to reveal the charge transfer in NiFeP.

Experiments were performed at BL5U of the UVSOR facility. $Ni_2P(10\text{-}10)$ and $Fe_2P(10\text{-}10)$ were cleaned by cycles of Ar^+ ion spattering (0.5 keV) and annealing (600 °C and 750 °C, respectively). The cleaned surfaces showed c(2x4) and c(2x2) LEED patterns, respectively. Fe (Ni) atoms were deposited on the Ni_2P (Fe_2P) clean surface at room temperature and the films were post annealed at 350 °C (550 °C), which induces phosphorization of the film owing to surface segregation of P atoms from the bulk [3,4]. The prepared Fe_xP/Ni_2P and Ni_xP/Fe_2P samples showed 1x2 and c(2x2) LEED patterns, respectively. Ni 3p, P 2p, Fe 3p and valence band photoelectron spectroscopy (PES) measurements were performed by an MBS A-1 analyzer.

The Fe 3p spectra of Fe_2P, Ni_xP/Fe_2P and Fe_xP/Ni_2P are shown in Fig.1 (a). The analyses of angle resolved Fe 3p spectra revealed that the 3p level of Fe atoms in the interface region of Ni_xP/Fe_2P located at 54.5 eV. This is slightly higher than that observed for a Fe_2P substrate. The Ni 3p spectra of Ni_2P, Ni_xP/Fe_2P and Fe_xP/Ni_2P are shown in Fig.1 (b). Ni 3p peak of Ni_xP/Fe_2P was shifted to the lower binding energy side from that of the Ni_2P substrate. The results showed that Fe 3p and Ni 3p peaks were shifted due to the interaction between the Ni_2P thin film and the Fe_2P substrate. On the other hand, these peaks showed little shifts in the case of Fe_xP/Ni_2P. These results suggest that the Ni_xP film is chemically bound to the Fe_2P substrate while the interaction between the film and the substrate is weak in the case of Fe_xP/Ni_2P.
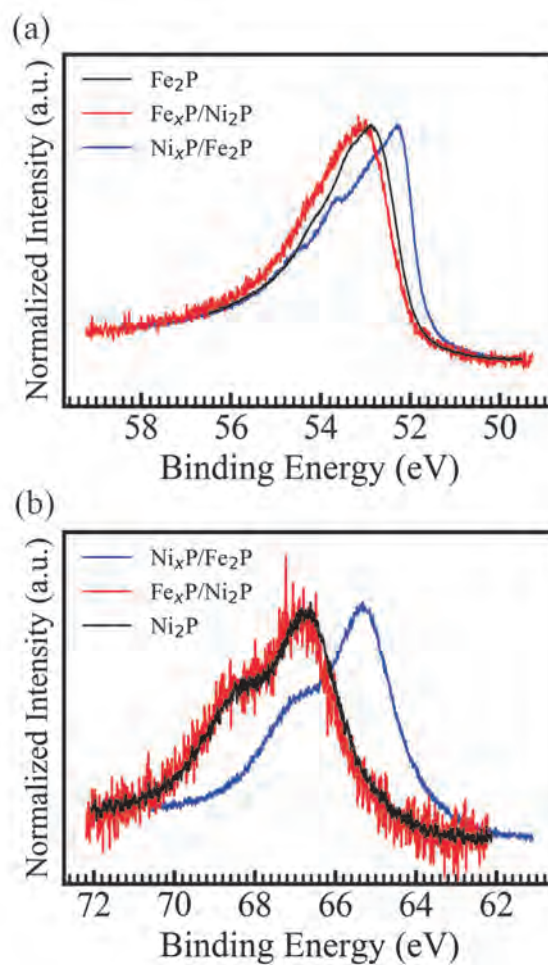

Fig. 1. (a) Fe 3p and (b) Ni 3p photoelectron spectra of Fe_2P, Ni_2P, Fe_xP/Ni_2P and Ni_xP/Fe_2P

[1] S. T. Oyama *et al.,* J.Catal. **216** (2003) 343.

[2] S. T. Oyama *et al.,* J.Catal. **285** (2012) 1.

[3] S. Imanishi *et al.,* e-J. Surf. Sci. Nanotech. **10** (2012) 45.

[4] Y. Sugizaki *et al.,* Jpn. J. Appl. Phys. **57** (2018) 115701.

BL5U

Electronic Band Structure of Novel Se-containing Phases on SrTiO₃

B. Lin[1,2], C. Y. Hong[1,2], Z. Song[1,2], P. X. Ran[1,2] and R.-H. He[2]

[1]*Department of Physics, Fudan University, Shanghai 200433, China*
[2]*School of Science, Westlake Institute for Advanced Study, Westlake University,*
Hangzhou 310064, China

Searching for novel quantum materials and understanding their properties have been a major theme in condensed matter physics. Se substitution in SrTiO₃ has revealed multiple electronic phases with peculiar band structures that were initially observed using our home-based ARPES with Helium lamp.

To further study the electronic band structure of one of the phases (Phase #1), we performed systematic ARPES measurements at the BL5U of UVSOR. A series of Fermi surface maps and cuts along high-symmetry directions were measured with photons of linearly horizontal (LH) and linearly vertical (LV) polarization and energy (hν) from 42 eV to 180 eV at T=5.8 K. Figures 1(a) and (b) are, respectively, an iso-energy contour and the band dispersion along Cut#1 through Γ point obtained with hν = 160 eV (LH). Figure 2 are Cut#1 taken with a series of photon energies between 57 eV and 67 eV with LH & LV polarization, which suggests a negligible kz dependence.

We also studied another phase (Phase #2) in Se-substituted SrTiO₃ that is different from the one above. Figure 3 compare the cuts measured near Γ point between Phase #1 and Phase #2 with hν = 60 eV at T = 5.8 K. Our measurements of Phase #2 show the photon energy dependence from 110 eV to 125 eV (See Fig. 4).

Fig. 2. Cut #1 in Fig. 1(a) measured with a series of photon energies between 57 eV and 67 eV with LH & LV polarization at T = 5.8 K.

Fig. 3. Band dispersion image measured with hν = 60 eV at T = 5.8 K for (a) Phase #1 and (b) Phase #2 along Cut #2 as marked in Fig. 3(c).
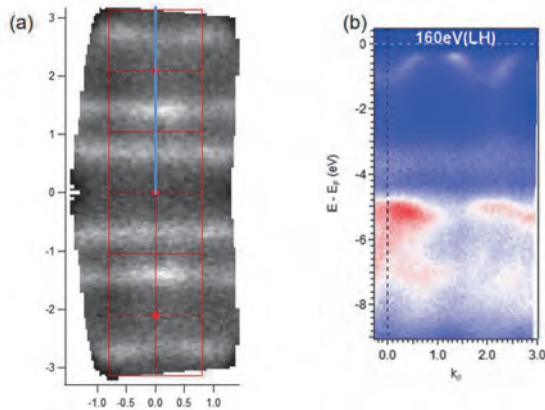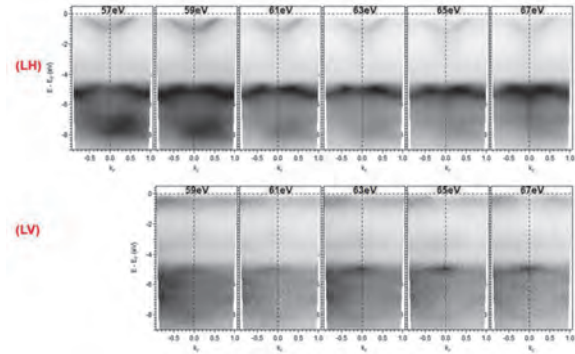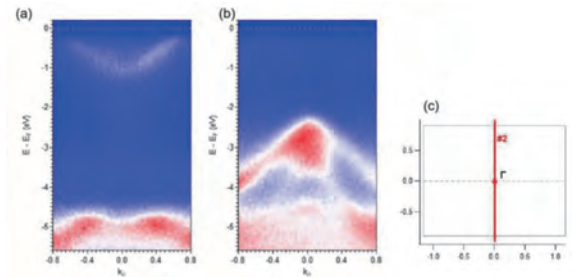

Fig. 1. Iso-energy contour and momentum cut obtained with hν = 160 eV at T = 5.8 K. (a) Integrated spectral intensity in the momentum space of Phase 1 over a small energy window [-0.21 eV, -0.19 eV]. (b) Band dispersion image along Cut #1 as marked in Fig. 1(a).
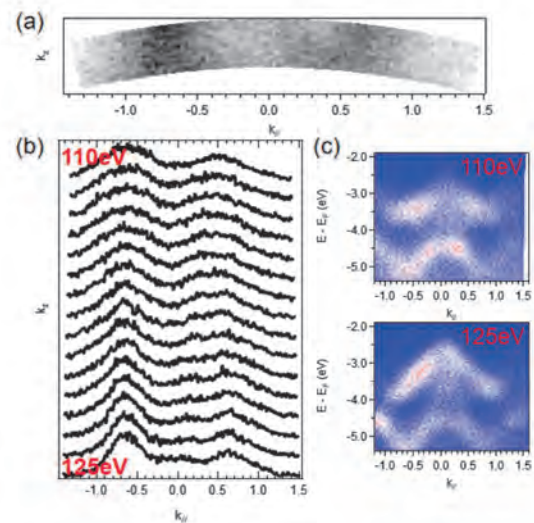

Fig. 4. kz dependence of Phase #2. (a) Iso-energy map in the k∥-kz plane and (b) stacked momentum distribution curves (MDCs) at energy -3.5eV. (c) Band dispersion image along Cut #2 as marked in Fig. 3(c) with hν = 110 eV & 125 eV.

BL5B

Reflectance Measurements of Al/TiO₂ Bilayers in the 10–30 eV Region at BL5B, UVSOR

T. Hatano[1], Y. Matsuda[2] and T. Ejima[1]

[1]IMRAM, Tohoku University, Sendai 980-8577, Japan
[2]Department of Chemistry, Graduate School of Science, Tohoku Universuty, Sendai 980-8578, Japan

VUV of a photon energy of 12.4 eV from Ar excited by laser pulse is a high potential source when it is focused by a suitable condenser optics. Al is known as the best material for normal incidence mirror if its surface is not covered by oxide layer. As a capping layer material to prevent the surface oxidization of Al, we have chosen TiO₂ considering its low refractive index at 12.4 eV, 0.63 [1]. By bilayer model of 2 or 4 nm thick TiO₂ on a thick Al, normal incidence reflectance can be expected as 68 % or 52 %, respectively. We have fabricated Al/TiO₂ bilayer on SiO₂ substrates by three methods: (1) Al (100 nm)/TiO₂ (2 and 4 nm) by consecutive thermal evaporation deposition, (2) Al (200 nm) thermal evaporation deposition, transfer to another vacuum chamber, Al surface oxide layer milling and TiO₂ (2 and 4 nm) magnetron sputtering deposition, and (3) Al (200 nm)/TiO₂ (0–14 nm gradient) consecutive ion beam sputtering deposition.

Reflectance measurements were performed at BL5B, UVSOR. The grating and mirror combination was G3M5. The angle of incidence was 11.6°.

Figure 1 shows the measured spectral reflectance of evaporated Al (100 nm)/TiO₂ (2 and 4 nm) bilayers. Oscillation structure appeared through 9–31 eV. The period did not depend on the thickness of TiO₂, which means the oscillation was caused by interference of substrate-Al interface reflection and Al-TiO₂ interface reflection. The spectral shape in 9–15 eV looks like a reduced-size copy of that in18–30 eV. It is because of the second order diffraction of the monochromator [2]. As a result, reflectances at 12.4 eV were quite low.

Figure 2 shows the measured spectral reflectance of evaporated Al (200 nm)/sputtered TiO₂ (2 and 4 nm) bilayers. The thickness of Al layer is uncertain because of the oxide layer removal before TiO₂ deposition. The result that the periods of the oscillation structure were shorter than those of Fig. 1 means the Al layer was thicker than 100 nm.

Figure 3 shows the measured spectral reflectance of sputtered Al (200 nm)/TiO₂ (0–14 nm) bilayer. Measurement points was shifted by 8 mm to change TiO₂ thickness by 2 nm. The plot raveled by 0 nm shows an Al with surface oxide layer. The reflectance in low energy region was unexpectedly low [3]. The reason could be attributed to the second and higher order diffraction or low energy scattering of the gating could be attributed.
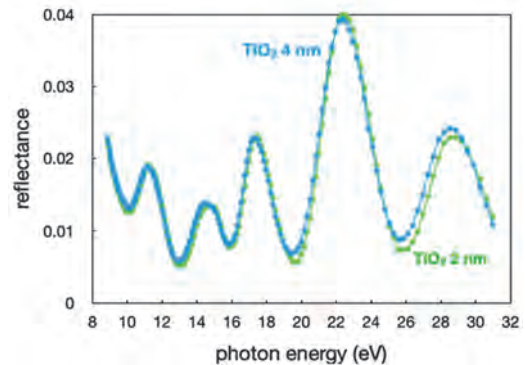

Fig. 1. Spectral reflectances of evaporated Al (100 nm)/TiO₂ (2 and 4 nm) bilayers.

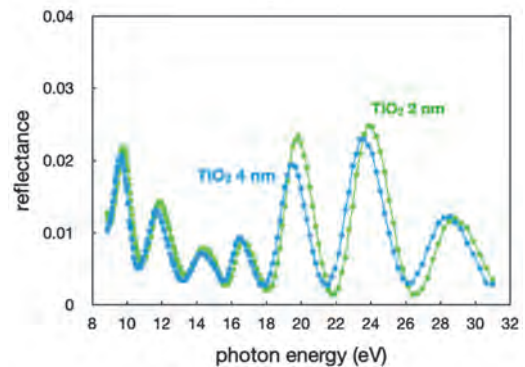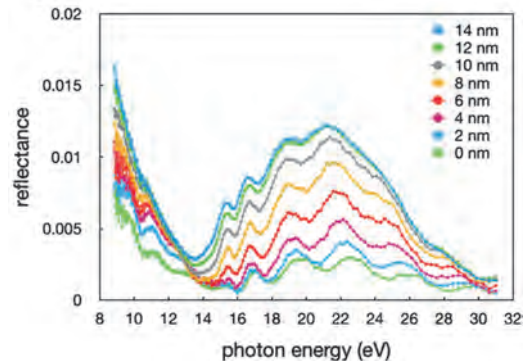Fig. 2. Spectral reflectances of evaporated Al (200 nm)/sputtered TiO₂ (2 and 4 nm) bilayers.

Fig. 3. Spectral reflectances of sputtered Al (200 nm)/TiO₂ (0–14 nm) bilayer.

[1] *Handbook of Optical Constants of Solids* (Ed. by Edward D. Palik, Academic Press, Inc., 1985).
[2] T. Hatano *et al*., UVSOR Activity Report 2019 **47** (2020) 41
[3] G. Hass and R. Tousey, J. Opt. Soc. Am. **49** (1959) 539.

Ⅲ-4

BL5B

Measurement of Soft X-Ray Resonant Magneto-Optical Kerr Effect for GdFe(Co) and TbFe

T. Sumi[1], M. Horio[1], S. E. Moussaoui[1], E. Nakamura[2], S. Makita[2], K. Tanaka[2,3],
A. Tsukamoto[4] and I. Matsuda[1]

[1]*The Institute for Solid States Physics, The University of Tokyo, Kashiwa 277-8581, Japan*
[2]*Institute for Molecular Science, Okazaki 444-8585, Japan*
[3]*the Graduate University for Advanced Studies, SOUKENDAI, Okazaki 444-8585, Japan*
[4]*College of Science and Technique, Nihon University, Funabashi 274-8501, Japan*

In the advanced information society today, spintronic devices have attracted great interests due to the fast-processing speed [1]. The material is complicated and composed of multi-element, it has been demanded to track their spin dynamics at individual magnetic elements. Recently, we have developed an experimental technique of the resonant magneto-optical Kerr effect (RMOKE) in soft X-ray region and succeeded in element-selectively tracing spin-states of d-electrons at transition metal atoms, *e.g.* Fe [1-5]. In the present research, we extended our spintronics research to the f-electronic system, such as in rare-earth elements, by the RMOKE experiment.

We prepared two ferrimagnetic samples: $Gd_{23}Fe_{67}Co_{10}$ crystal and $Tb_{20}Fe_{80}$ crystal. The direction of spontaneous magnetization was perpendicular to the surface. The experiments were carried out at soft X-ray beamline BL5B. The beam is irradiated on the sample with an angle of 67.5 degrees with respect to the surface normal. The specular beam after the reflection was led to a unit of the rotating analyzer ellipsometry (RAE) for analyses of the light polarization, *i.e.* the Kerr rotation angle. The RAE system was composed of a multilayer mirror and a detector of microchannel plate. By rotating the unit with respect to the beam direction, the Kerr rotation angle θ_k was determined by $\theta_K = -(\chi_+ - \chi_-)/2$, where χ_+ and χ_- are the rotation angle which is the measured at the intensity maximum of the ellipsometry curves under the positive and negative magnetic field, respectively.

Figure 1 shows photon energy spectra of the Kerr rotation angle for crystals of $Gd_{23}Fe_{67}Co_{10}$ and $Tb_{20}Fe_{80}$. The degree of Kerr rotation angle corresponds to magnetizations at each element. Therefore, we found that the spin directions of f-electrons system are opposite to those of d-electrons system in both GdFe(Co) and TbFe. This result is consistent to the spin configuration in a ferrimagnetic material and it demonstrates that our RMOKE can be applied to the f-electronic systems.
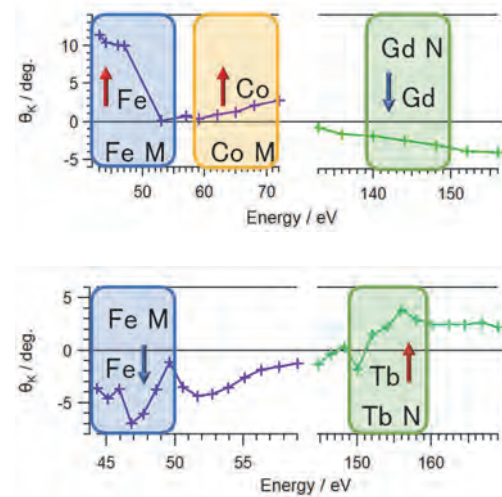
Fig. 1. Photon energy dependence of Kerr rotation angle for crystals of (top) $Gd_{23}Fe_{67}Co_{10}$ and (bottom) $Tb_{20}Fe_{80}$ crystal. The solid squares correspond to the absorption edge of each elements.

[1] C. D. Stanciu *et. al.,* Phys. Rev. Lett. **99** (2007) 047601.
[2] Sh. Yamamoto *et. al.,* Phys. Rev. B **89** (2014) 064423.
[3] Sh. Yamamoto and I. Matsuda, Appl. Sci. **7** (2017) 662.
[4] Sh. Yamamoto *et. al.* Rev. Sci. Instrum. **86** (2015) 083901.
[5] K. Yamamoto *et. al.* Appl. Phys. Lett. **116** (2020) 172406.

BL6U

Domain Distribution in the Monolayer CVD Graphene Sheet Observed with Photoelectron Momentum Microscope

Y. Aoyagi[1], S. Ohno[1] and F. Matsui[2]

[1]*Graduate School of Engineerig Science,Yokohama National University, Yokohama 240-8501, Japan*
[2]*UVSOR Synchrotron Facility, Institute for Molecular Science, Okazaki 444-8585, Japan*

Photoelectron Momentum Microscope (MM) is considered as a promising means to explore orbital tomography of organic molecules as well as various nanostructures such as a graphene nanolayer [1]. In the present work, we focused on the graphene monolayer produced by chemical vapor deposition (CVD) and subsequently transferred to the silicon oxide substrate.

Experiments were performed at BL6U of UVSOR III. Band dispersion data of CVD monolayer graphene were obtained over a wide reciprocal range. Figure 1 shows the typical result obtained near Fermi level. This indicates that a single-domain structure is formed within the accuracy of the spatial resolution of the present measurements. Based on this type of the data, we can easily recognize the orientation of the monolayer graphene sheet. In contrast, we observed ring-like pattern at some part of the sample. We deduce that several domains coexist at such a position. In other words, density of the domain boundary is larger, resulting in the isotropic electronic states within the monolayer graphene sheet at such a location. In order to clarify further the two-dimensional distribution of the single-domain structure, we conducted the measurements of the two-dimensional mapping as shown in Fig. 2. We found that single-domain with several equivalent directions coexist within the measured area (70 x 500 μm^2). This indicates that there should be a preferred direction of the domain boundary line between the single-domain structures. Our atomic force microscopy (AFM) study showed that many boundary lines should exist inside of the single-domain region, although the band dispersion is well retained as shown in Fig. 1. Our present results indicate that the macroscopic self-organization process should exist during the growth of CVD monolayer graphene sheet so that the three single-domain structures preferentially coexist in a macroscopic range. We deduce that not only the local electronic structure at the atomic scale but also that at the submicron scale should be assessed more carefully to grasp the spatial distribution of the domains with a typical band dispersion or isotropic electronic state.

In the study of two-dimensional materials, it is well recognized that the effect related to the domain boundary should be carefully assessed [2]. Here, we propose that MM will become a useful means to relate the microscopic knowledge with macroscopic transport property and other physical properties.
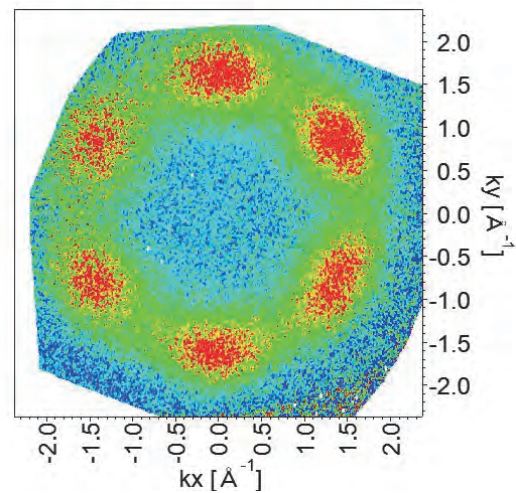

Fig. 1. Isoenergy cross section of the valence band dispersion of CVD graphene monolayer near Fermi level. Photoelectron peaks appeared at the K points.
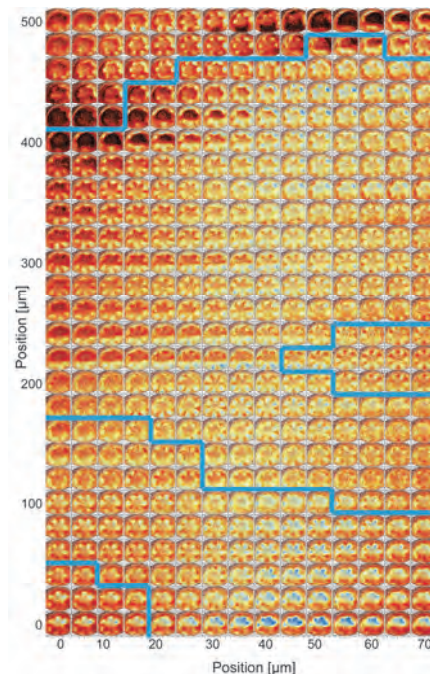

Fig 2. The Fermi surface patterns from two-dimensionally scanned positions.

[1] F. Matsui *et al.*, Jpn. J. Appl. Phys. **59** (2020) 067001.
[2] S. M. Hus *et al.*, Prog. Surf. Sci. **92** (2017) 176.

Ⅲ-4

BL6U

Electronic Structures of 1T-TaS$_2$ Studied by a Momentum Microscope

S. Suga[1], T. Kobayashi[2], E. Iwamoto[2], K.Sakamoto[2] and F. Matsui[3]

[1]ISIR, Osaka University, Ibaraki 567-0047, Japan
[2]Graduate School of Engineering, Osaka University, Suita 565-0871, Japan
[3]UVSOR Synchrotron Facility, Institute for Molecular Science, Okazaki 444-8585, Japan

Among various transition metal dichalcogenides, 1T-TaS$_2$ shows the richest phase diagram including a pronounced metal to insulator phase transition (MIT) and a sequence of different charge density wave (CDW) transformation. With lowering temperatures, incommensurate CDW (ICCDW) is observed below 550K and then nearly commensurate phase (NC- CDW) is seen below 350 K. Further a commensurate CDW (CCDW) is realized below 180 K.

This material is cleaved in UHV and the angle resolve photoemission spectra in a wide wave vector space were measured at various E$_B$ by use of synchrotron radiation (SR) by a newly installed momentum microscope (MM) at BL6U of UVSOR.

The advantage of MM is that without any rotation of the sample, photoemission intensity at more than several thousand multichannels of wide (k$_x$,k$_y$) can be simultaneously recorded by a 2D detector in the form of E$_B$(k$_x$,k$_y$). Therefore the sample-rotation dependent intensity normalization, slight shift of the measured area on the sample surface as well as the consideration of the change of the measurement configurations are not at all required for analyses.

As soon as a flat and clean sample surface is obtained, one should locate the sample just in front of the PEEM objective lens by use of delicate sample manipulator. Then one can obtain huge amount of data set within a short time. Partial results are shown in Figs. 1 (a)-(d). These results are obtained at T=50 K in the CCDW phase by use of monochromatized synchrotron radiation light at hν=66 eV. The binding energies E$_B$ correspond to (a) 0 eV, (b) 0.5 eV, (c) 1.0 eV and (d) 1.5 eV. Each data is integrated within ± 0.15 eV for realizing enough statistics.

The detailed behavior of the Ta 5d orbitals is clearly recognized around the k$_x$=0, k$_y$=0 point in the data (a)-(c). Since even the 2nd Brillouin zone is imaged, the hole pocket resulting from the S 3p orbital can be recognized in Fig(d) near k$_x$=0, k$_y$=2Å^{-1}.

The band dispersions can be then easily revealed not only along the k$_y$ axis but also any k$_x$-k$_y$ axes by comparing the data selected from a huge data set integrated at different temperatures.

Thus high potential of MM for studying detailed I(E$_B$(k$_x$,k$_y$)) is clarified [1]. I(E$_B$(k$_x$,k$_y$,k$_z$)) measurement is also possible by use of SR.

[1] S. Suga, A. Sekiyama and C. Tusche, Photo-electron Spectroscopy, Springer Series in Surface Sciences **72** (2021), in press.
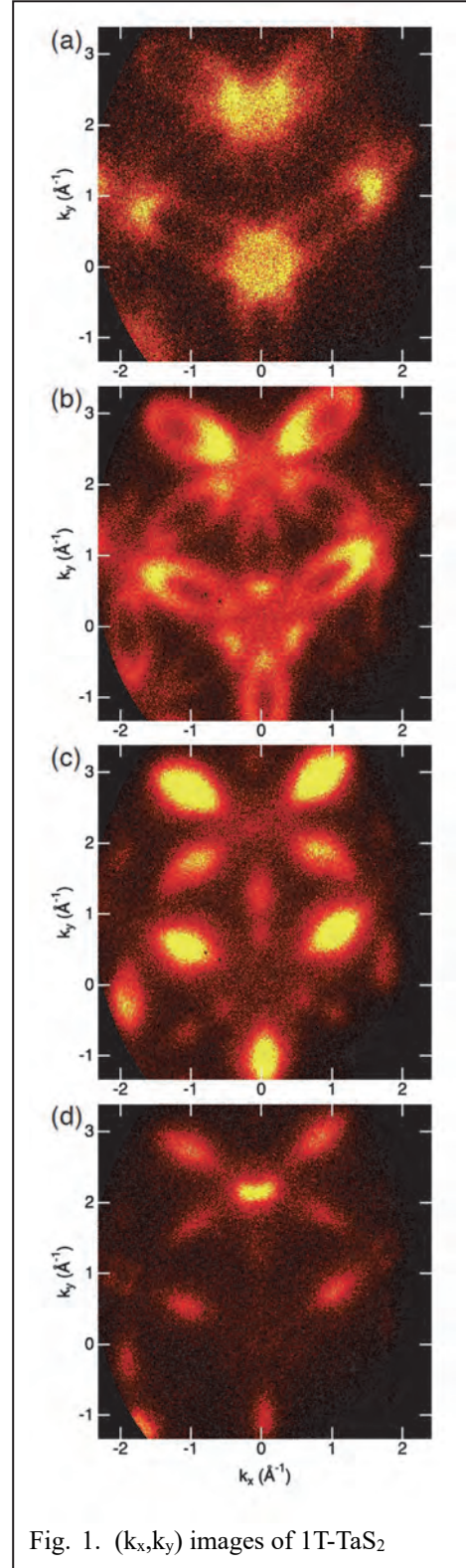
Fig. 1. (k$_x$,k$_y$) images of 1T-TaS$_2$

BL6U

Momentum Microscopy of Highly Oriented Dph-BTBT Film on Ag(110)

M. Iwasawa[1], Y. Hasegawa[2], F. Matsui[3], S. Kera[3] and Y. Yamada[1]

[1]Faculty of Pure and Applied Sciences, University of Tsukuba, Tsukuba 305-8573, Japan
[2]Institute for Molecular Science, Okazaki 444-8585, Japan
[3]UVSOR Synchrotron Facility, Institute for Molecular Science, Okazaki 444-8585, Japan

While devices based on [1]benzothieno[3,2-b] [1] benzothiophene (BTBT) derivatives, which exhibit strong intermolecular interactions and atmospheric stability, have achieved mobility in excess of 30 cm^2/Vs, the origin of their efficient conduction is still not fully understood. Although the mobility of many organic semiconductors has been understood by the energy and spatial distribution of HOMO, a recent study has shown that the contribution of HOMO-1 is significant in BTBT derivatives [1]. In this study, we focused on Dph-BTBT, one of the BTBT derivatives, and analyzed the energy states and the photoelectron angular distribution (PAD) of HOMO and HOMO-1.

For the detailed measurement and the analysis of PAD, a molecular layer with single domain structure is required. We have recently shown that well-ordered Dph-BTBT film can be realized on metal(111) surface [2]. However, Dph-BTBT film on metal(111) has multi-domain structure, which is not suitable for the PAD measurement. Therefore, we have further demonstrate that, by using anisotropic Ag(110) surface, a nearly one-dimensionally oriented film of Dph-BTBT can be fabricated. Here, we tried to measure the photoelectron momentum map of the single-domain, multilayer film of Dph-BTBT on Ag(110).

The one-dimensionally oriented Dph-BTBT film were fabricated by supplying 10 nm of Dph-BTBT on clean Ag(110). The molecular structure of the Dph-BTBT film was examined using a scanning tunneling microscope (STM) and low energy electron diffraction (LEED). The PAD measurements were performed using momentum microscope at BL6U of UVSOR.

Figure 1 shows the STM image and LEED pattern of Dph-BTBT film on Ag(110). It is seen that the molecular long axis is almost along with the [1-10] direction of the substrate, indicating the formation of nearly one-dimensional structure. Although it was not a completely single-domain structure, it is a suitable sample for the measurement of PAD.

Figure 2(a) shows the energy distribution curve (EDC) of Dph-BTBT film on Ag(110). It is found that both HOMO and HOMO-1 are energetically broadened. Here, each orbital can be fitted with two Gaussian functions, suggesting that orbital splitting due to the overlap of neighboring (upper and lower) molecules. Then, we examined PAD patterns of each orbital as shown in Fig. 2(b, c). It is recognized that both PAD patterns of HOMO and HOMO-1 have strong intensity in kx direction, which is in general agreement with the simulation by means of FFT of molecular orbital. For the detail analysis, we focus on the energy dependance

of the peak location and the width at half maximum (FWHM) of the intensity at around kx = 1.5 ~ 1.7 Å^{-1} as illustrated with arrows in Fig. 2(b). As for the peak location (blue dots in Fig. 2(a)), there is no change in the HOMO region, but a gradual shift to the lower-momentum side is seen in the HOMO-1 region. On the other hand, the FWHM shows little change in the kx direction (orange dots), but a significant change in the ky direction (green dots) in the HOMO region.

Thus, by means of PAD using the momentum microscope at BL6U, we were able to experimentally detect the subtle changes in the wavefunction of Dph-BTBT in the condensed state, which was difficult by the conventional techniques.
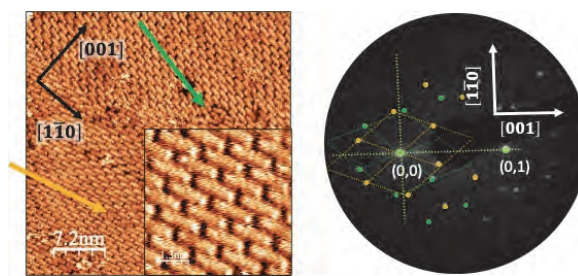

Fig. 1. STM image and LEED pattern of Dph-BTBT/Ag(110).
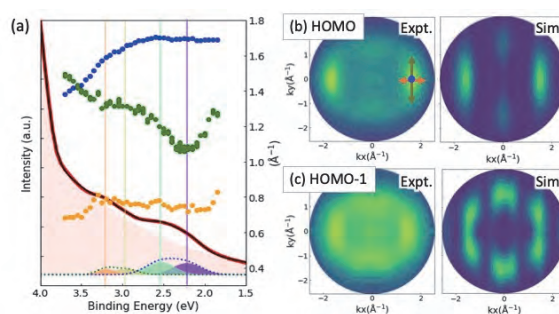

Fig. 2. (a) EDC plotted with peak location and FWHM of PAD. (b, c) PAD patterns of HOMO and HOMO-1 of Dph-BTBT.

[1] Y. Kuroda *et al.,* Jpn. J. Appl. Phys. **58** (2019).
[2] Y. Yamada *et al.,* UVSOR Activity Report 2019 **47** (2020) 137.

Ⅲ-4

BL6U

PEEM-mode Magnification Parameters
for Photoelectron Momentum Microscopy

F. Matsui[1], S. Makita[1], H. Matsuda[1], Y. Okano[1], T. Yano[1], E. Nakamura[1] and S. Kera[1,2]

[1]UVSOR Synchrotron Facility, Institute for Molecular Science, Okazaki 444-8585, Japan
[2]The Graduate University for Advanced Studies, SOKENDAI, Okazaki 444-8585, Japan

As reported in the previous activity report, new experimental station for momentum microscopy was constructed and is currently operating at the BL6U, an undulator-based soft X-ray beamline [1,2]. The photoelectron momentum microscope is a unique multifunctional system for characterizing the electronic properties of μm- and nm-scale structures. A spectro-microscopy (PEEM) mode in real space and micro-spectroscopy (momentum) mode in reciprocal space are available.

Calibration and lens parameter optimization are important issues for high quality data acquisition, so we use checkered-patterned samples for this purpose.

The spatial distribution of elements can be mapped using photoelectrons from the core level. On the other hand, the contrast in valence photoelectron images varies from case to case. In a recent paper [3], we reported on a detailed study of contrast formation. The photoelectron intensity of the gold region near the Fermi level was higher than that of the silicon substrate region, while the inverted contrast images were obtained at lower kinetic energies. The contrast inversion in the photoelectron images by mercury (Hg) lamp excitation is due to the differences in work functions specific to materials and surface conditions, and that of synchrotron radiation excitation is due to the difference in the density of states between gold and silicon substrate.

The following is an overview of the magnification modes available in PEEM mode. Figure 1 shows an example of observing a checkerboard pattern in various magnification modes. Hg lamp excitation was used. The largest field of view (φ 140 μm) is achieved by Mag.1 mode. Note that the irradiation spot on the sample is smaller than the field of view in the present case. The intensity ratios of different magnifications are indicated together. In higher magnification modes, the flux density per pixel is reduced, resulting in lower photoelectron intensity. Since the momentum of photoelectrons excited by the Hg lamp is smaller than the acceptance cone of the PEEM lens, all photoelectrons are detected. In the case of synchrotron radiation excitation, it is needed to considered that the acceptance cone in the momentum space limits the photoelectrons in low magnification mode.

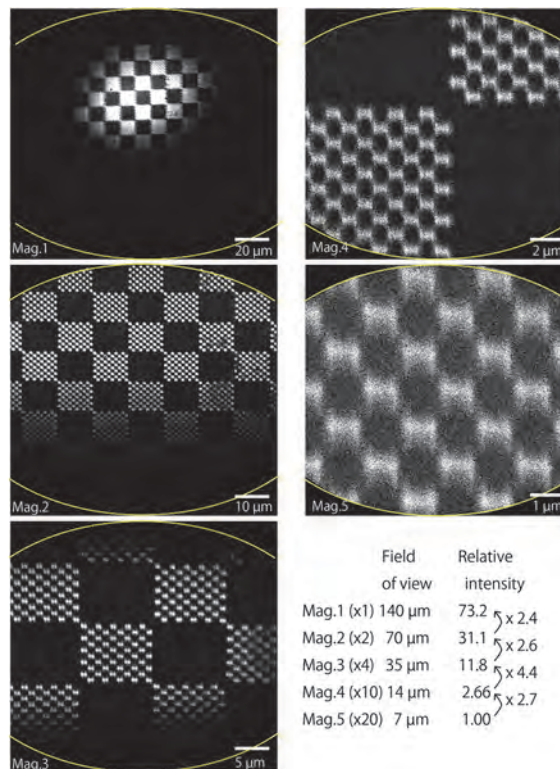|	Field of view	Relative intensity	
Mag.1 (x1)	140 μm	73.2	⤸ x 2.4
Mag.2 (x2)	70 μm	31.1	⤸ x 2.6
Mag.3 (x4)	35 μm	11.8	⤸ x 4.4
Mag.4 (x10)	14 μm	2.66	⤸ x 2.7
Mag.5 (x20)	7 μm	1.00	⤸

Fig. 1. A checkered pattern observed by the photoelectron momentum microscope in various magnification modes. The Hg lamp was used for excitation.

[1] F. Matsui S. Makita, H. Matsuda, T. Yano, E. Nakamura, K. Tanaka, S. Suga, and S. Kera, Jpn. J. Appl. Phys. **59** (2020) 067001.
[2] F. Matsui, S. Makita, Y. Okano, H. Matsuda, and S. Kera, Vacuum and Surface Science accepted (2021).
[3] S. Makita, H. Matsuda, Y. Okano, T. Yano, E. Nakamura, Y. Hasegawa, S. Kera, S. Suga, and F. Matsui: e-J. Surf. Sci. Nanotech. accepted (2021).

Ⅲ-4

BL7U

Study of Electronic Band Structure of Li- and Ca-Intercalated Graphene

S. Ichinokura[1], M. Hashizume[1], K. Horii[1], R. Fukushima[1], M. Toyoda[1], S. Ideta[2],
K. Tanaka[2], R. Shimizu[3], T. Hitosugi[3], S. Saito[1] and T. Hirahara[1]

[1]Department of Physics, Tokyo Institute of Technology, Tokyo 152-8551, Japan
[2]UVSOR Synchrotron Facility, Institute for Molecular Science, Okazaki 444-8585, Japan
[3]Department of Applied Chemistry, Tokyo Institute of Technology, Tokyo 152-8550, Japan

Graphene is known as the most promising nanomaterial for the post-silicon electrical industry. The remarkable high-carrier mobility in graphene originates from its characteristic band structure called the Dirac cone. When the Fermi energy in graphene locates near the Dirac cone crossing (Dirac point), graphene has a massless carrier due to its linear and steep band dispersion.

Many-body interaction in graphene materials is also a target of intensive research. The band structure of monolayer graphene has a saddle point at the M point of the Brillouin zone. The dispersion near this point is flat, leading to the heavy effective mass and divergent density of states. This is called Van Hove singularity (VHS), expected to drive unconventional superconductivity. It is known that deposition of alkali- and alkaline earth-metals tunes the Fermi energy to the VHS point upon electron doping [1,2]. Recently, this VHS filling has attracted renewed interest due to the emergence of superconductivity in twisted bilayer graphene, which also originated from the VHS at the Fermi level [3].

In our group, a comprehensive study on alkali- and alkaline earth-doped graphene is carried out by a combination of *in situ* angle-resolved photoemission spectroscopy (ARPES) and electrical transport measurements in ultrahigh vacuum (UHV). By comparing band structures and the transport properties, we are investigating the many-body interaction in graphene.

In the present study, we prepared monolayer graphene on SiC(0001) substrates. Li and Ca were doped by vapor deposition and annealing in UHV, followed by *in situ* ARPES measurements. In Fig. 1, we show the band structure of (a) as-grown, (b) Li- and (c) Ca-doped graphene. The Brillouin zone (BZ) of the graphene is drawn in Fig. 1(d). Fig. 1(a) was collected around K point, parallel to the direction shown as the solid green line in Fig. 1(d). The slightly n-doped single Dirac cone centered at the K point is seen, typical for the monolayer graphene. On SiC, such high-quality epitaxial growth of graphene is possible because of the underlying buffer layer, which terminates the dangling bonds of the SiC(0001) surface.

Figures 1(b) and (c) were taken at the Γ point along the Γ-K line, shown as the solid magenta line in Fig. 1(d). In both spectra, steep band dispersions are seen. We conclude that these bands are two pairs of Dirac bands (denoted as π_1^* and π_2^*). In Ref. [4], it was reported that Li intercalates into both sides of the buffer layer. Consequently, the atomic structure of the

system is changed into a layered one shown in Fig. 1(e); Li terminates the substrate dangling bonds and decouples the buffer layer from the substrate. Further deposited Li intercalates between the lifted graphene and the top one, forming the √3×√3 periodicity. The heavily-doped two Dirac bands observed around Γ in Fig. 1(b) perfectly match this picture. Besides, the π_2^* band reaches the Fermi level at its flat part at the M point of √3×√3 BZ, which satisfies the VHS.

We newly found that similar structural change takes place in Ca-doped graphene, with further charge transfer to π_1^* and π_2^* bands. In Fig. 1(c), another band with a parabolic shape can be seen. This free-electron (FE) like characteristic corresponds to the interlayer band of superconducting Ca-intercalated graphite [5].
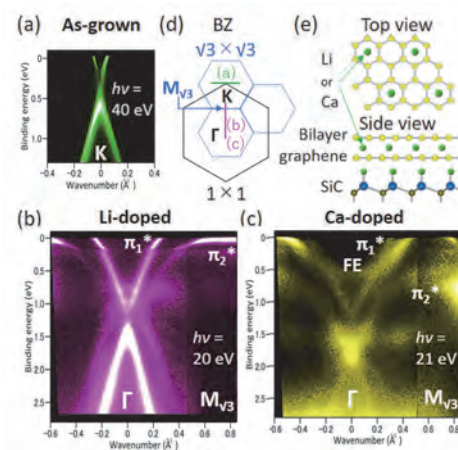

Fig. 1. (a)-(c) Band structure of (a)As-grown, (b) Li-doped and (c) Ca-doped graphene. ARPES measurements were performed with hν= 20-40 eV p-polarized light under T = 11-13 K. (d) Schematic of 1×1 and √3×√3 BZ. Measurement directions of (a)-(c) are drawn as solid green and magenta lines. (e) Schematic atomic model of Li- and Ca-doped graphene.

[1] J. L. McChesney *et al.*, Phys. Rev. Lett. **104** (2010) 136803.
[2] P. Rosenzweig *et al.*, Phys. Rev. Lett. **125** (2020) 176403.
[3] Y. Cao *et al.*, Nature **556** (2018) 43.
[4] S. Fiori *et al.*, Phys. Rev. B **96** (2017) 125429.
[5] K. Sugawara *et al.*, Nat. Phys. **5** (2009) 40.

BL7U

Low-kinetic Energy and Low-temperature Measurements to Unveil the Impact of Weak Interaction: a Machine Status of the BL7U

Y. Hasegawa[1], S. Ideta[1], K. Tanaka[1,2] and S. Kera[1,2]

[1]*Department of Photo-molecular science, Institute for Molecular Science, Okazaki 444-8585, Japan*
[2]*School of Physical Sciences, The Graduate University for Advanced Studies, SOKENDAI, Okazaki 444-8585, Japan*

The purpose of this study is to clarify the impacts on the electronic state of the organic/inorganic interface stabilized by weak interaction such as van der Waals force. We have studied the oriented-monolayer film of pentacene on graphite so far and realized the emergence of a dispersive band utilizing low-energy excitation angle-resolved photoelectron spectroscopy (LE-ARPES). The dispersive band appears at the kinetic energy of 1 to 2 eV where the secondary electron is a non-negligible and constant final state (CFS) feature is overlapping with the non-dispersive molecular orbital states. The CFS band could be originated from a newly-formed conduction band at the weakly bounded interface visualized by high-resolution angle-resolved secondary electron emission [1], demonstrating that the impact of weak interaction would appear much stronger in unoccupied states by a larger spread of an electron cloud. During the experiment at BL7U, however, we encountered technical issues to measure this system at low-kinetic energy and low temperature this time.

A single crystalline graphite (SCG) as the substrate was cleaned by annealing at 600 K for 2 h. A pentacene film of 4.1 Å was deposited onto the SCG at room temperature in a custom UHV chamber designed for organic layer deposition. After the deposition, a rapidly cooled sample below the phase transition temperature [2] was measured.

Figure 1 shows LE-ARPES image of the SCG taken at hν of 7.4 eV on the same day. In the image, the signal lacks at the lower right, and the energy and angle positions are different from each other. There was no choice to optimize the image distortion properly by arranging the experimental setup, a measurement position, a sample preparation, and so on. This curve appears nearly the same position at a different excitation energy of 7.2 eV and 8.0 eV because the photoemission is mainly from a secondary electron. This kind of time-dependent phenomenon has never been found at BL7U, therefore, the artifact was caused by changes of the present analyzer condition, unfortunately.

Figure 2 shows ARPES of pentacene/SCG taken at hν = 40 eV with decreasing the temperature from 50 K to 10 K. Upon the cooling, a new feature appears at around binding energy of -11 eV at 10 K. According to the previous report, it is caused by adsorbing Ar atoms on the surfaces [3]. Evolution of the Ar 3p peak with the cooling is observed and the feature is completely recovered at 50 K by annealing (not shown). The molecular film structure (packing or orientation) is easily affected by adding such a weak perturbation of the gas adsorption [4]. To discuss the modification of the

electronic state of the molecular interfaces by the weak interaction, the low-temperature experiments are mandatory to monitor the effects of decreasing the distance between a molecule and the surface. We will improve the present machine status at BL7U for standing a severe experiment.
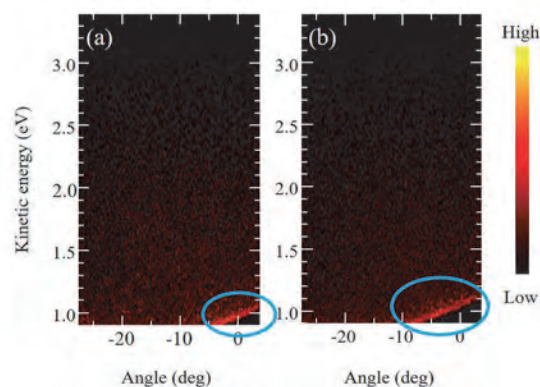

Fig. 1. (a) and (b) are LE-ARPES images of the same SCG taken at hν = 7.4 eV which show different lacked areas indicated by blue ovals.
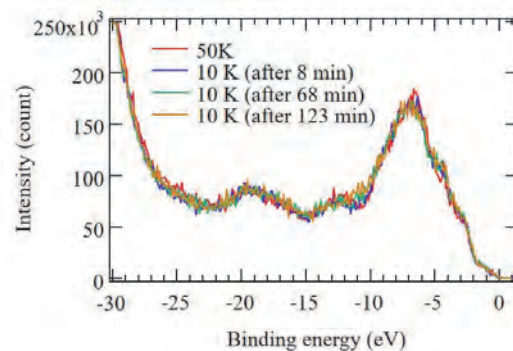

Fig. 2. ARPES spectra of pentacene/SCG measured with decreasing the temperature.

[1] T. Yamaguchi *et. al.*, UVSOR Activity Report 2018 **46** (2019) 148.
[2] Y. Hasegawa *et. al.*, UVSOR Activity Report 2019 **47** (2020) 140.
[3] F. Carnovale *et. al.*, J. Chem. Phys. **90** (1989) 1452.
[4] F. Bussolotti *et. al.*, Phys. Rev. Lett. **110** (2013) 267602.

Ⅲ-4

BL7U

Hybridization between π Band of Graphene and 6sp Band of Hex-Au(001) Reconstructed Structure

T. Terasawa[1,2], S. Tanaka[3], K. Matsunaga[4], T. Ito[4,5], S. Yasuda[1], S. Machida[1],
M. Yano[1] and H. Asaoka[1]

[1]*Advanced Science Research Center, Japan Atomic Energy Agency, Tokai 319-1195, Japan*
[2]*Institute of Industrial Science, The University of Tokyo, Tokyo 153-8505, Japan*
[3]*The institute of Scientific and Industrial Research, Osaka Univ., Ibaraki 567-0047, Japan*
[4]*Graduate School of Engineering, Nagoya University, Nagoya 464-8603, Japan*
[5]*Nagoya University Synchrotron radiation Research center (NUSR), Nagoya University, Nagoya 464-8603, Japan*

The interface between graphene and Au has attracted much attention since the large Rashba splitting of 100 meV in the π band of graphene/Au/Ni structure was discovered in 2012 [1]. As one of the graphene and Au interfaces, graphene on Hex-Au(001) reconstructed surface has also been studied. The quasi-one-dimensional periodic potential in this structure is considered to replicate graphene π band to open a new bandgap at the Brillouin zone boundary [2]. However, the electronic structure of this system has not been reported yet. In this study, we have performed angle-resolved photoemission spectroscopy (ARPES) on graphene grown on the Hex-Au(001) surface to directly investigate this system's electronic structure.

Graphene was prepared on Hex-Au(001) substrate using chemical vapor deposition in Japan atomic energy agency [3]. Hex-Au(001) spontaneously formed during the graphene growth. Low energy electron diffraction measurements indicated that the sample surface and the interface were unchanged during the transport under ambient conditions. ARPES measurements were performed at the UVSOR-III BL7U after the sample annealing in the pre-chamber by an IR-heater. Data were acquired at room temperature with $h\nu = 9 - 40$ eV. We changed the photon energy and polarization to visualize graphene and Au bands and their replicas.

Figure 1 shows the ARPES image on a Γ-X(Au)-K (graphene) line. Two sharp bands and one faint band were observed. The linear band dispersion from k = 1.7 Å^{-1} (K point of graphene) was assigned to the graphene π band. This band shows a mini-gap at the binding energy of about 0.9 eV. The other linear band crossing the Fermi energy at k = 1.2 Å^{-1} close to the X point of Au was assigned to the Au 6sp band, according to the previous report about the electronic structure of Hex-Au(001) [4]. An electron pocket around the X point was also consistent with the previous report [4].

The faint linear band comes from k = 1.47 Å^{-1} at the Fermi energy and crosses the top edge of the mini-gap. This band crossing suggests that this linear band is the origin of the mini-gap formation in the graphene π band. Accounting for the periodicity of the Hex-Au(001) surface of 1.44 nm, the reciprocal vector of this structure is 0.44 Å^{-1} [2,4]. Thus the original band of this band should begin from k = 1.47 ± n×0.44 Å^{-1}

at the Fermi energy. While this value does not match the graphene K point, k = 1.7 Å^{-1}, k = 1.47 - 0.44 = 1.03 Å^{-1} is reasonable for the Au 6sp band. Such the replicated Au 6sp band was observed for Hex-Au(001) in the previous report [4]. We concluded that the Au 6sp band hybridized with the graphene π band to form the mini-gap in the graphene π band. We expect this hybridization changes the electronic structure and the spin characteristics of graphene, similar to the hybridization between graphene and Au in the graphene/Au/Ni system reported in 2012 [1].
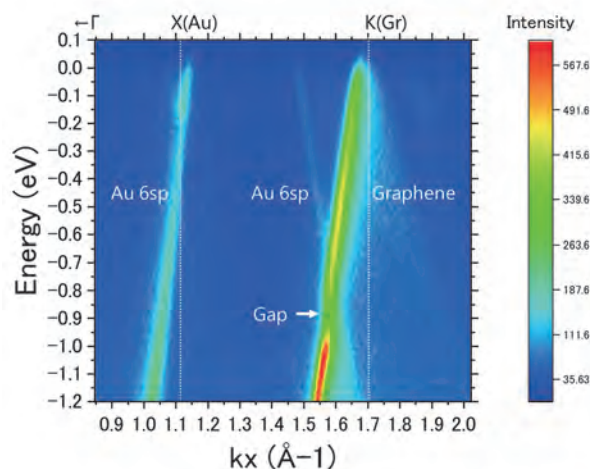

Fig. 1. Band structure of graphene grown on hex-Au(001) substrate. An energy gap of 150 meV was observed in the graphene π band.

[1] D. Marchenko, *et al.*, Nat. Commun. **3** (2012) 1232.
[2] X. Zhou, *et al.*, ACS Nano **10** (2016) 7550.
[3] T. Terasawa, *et al.*, Jpn. J. Appl. Phys. **58** (2019) SIIB17.
[4] S. Bengió, *et al.*, Phys. Rev. B **86** (2012) 045426.

Ⅲ-4

Topological Electronic Structure of the Interface between α-Sn and InSb

T. Nakaya[1], Y. Ohtsubo[2,1], T. Nakamura[1] and S. Kimura[2,1,3]

[1]Department of Physics, Graduate School of Science, Osaka University, Toyonaka 560-0043, Japan
[2]Graduate School of Frontier Biosciences, Osaka University, Suita 565-0871, Japan
[3]Department of Materials Molecular Science, Institute for Molecular Science, Okazaki 444-8585, Japan

Among the topological materials [1], α-Sn [2,3] is gathering much attention because of its possible spintronic application, as reported to exhibit spin to charge conversion due to the inverse Edelstein effect even at room temperature [4]. The next barrier for the new-generation spintronic devices is to realize the interface between TIs and normal semiconductors in order to make the spin-polarized topological electronic states available for them. Along this line, to make the junction between TI and normal semiconductor hosting the topological "interface" state is awaited. In this study, we have tried to grow normal semiconductor InSb, which has a small lattice mismatch to a topological material α-Sn (0.14%), on α-Sn(111) ultrathin films and observed its surface and interface electronic structure by angle-resolved photoelectron spectroscopy (ARPES).

The InSb(111) substrates were cleaned by repeated cycles of Ar+ sputtering (0.5 keV) and annealing up to 600 K in an ultra-high vacuum chamber. Then, homo-epitaxial growth of InSb was performed to obtain the clean surface of the InSb(111) substrates. α-Sn films with the thickness of 8 bi-atomic layers (BL) were obtained by evaporating Sn from a home-made evaporator. The evaporation rates of In, Sb, and Sn were monitored *in-situ* from the intensity oscillation of the electron diffraction patterns. After the growth, (1×1) periodic structure of α-Sn was observed, consistent with the earlier report [6]. On such α-Sn(111) films, In and Sb were deposited and the InSb layer with the thickness of ~1BL was grown there. The surface periodicity remained after the growth of InSb without in-plane lattice distortion.

Figure 1 shows the band dispersion of the InSb(~1BL)/α-Sn(8BL)/InSb(111)B observed by ARPES. A linear Dirac cone like dispersion (guided by dashed white lines), which is a typical behavior of the topological electronic states, was observed around the center of the surface Brillouin zone ($k_\chi = 0.0$Å^{-1}) after the deposition of the InSb layer. This result suggests that the topological surface state of α-Sn is transplanted to the interface with InSb, a normal semiconductor. Further analysis to understand the spin texture of the interface electronic states between α-Sn and InSb is in progress.

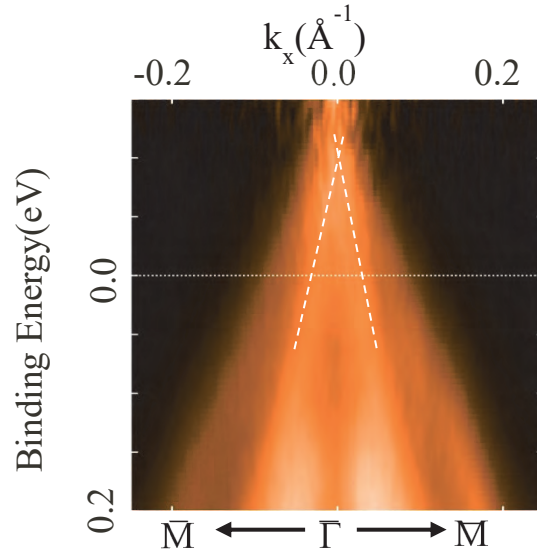Fig. 1. Band dispersion of InSb/α-Sn/InSb(111)B by observed by ARPES (hν = 16eV). The measurement was taken at room temperature and normalized by the Fermi distribution function.

[1] M. Z. Hasan and C. L. Kane, Rev. Mod. Phys. **82** (2010) 3045.
[2] Y. Ohtsubo *et al*., Phys. Rev. Lett. **111** (2013) 216401.
[3]A. Barfuss *et al*., Phys. Rev. Lett. **111** (2013) 157205.
[4] J-C Rojas-Sanchez *et al*., Phys. Rev. Lett. **116** (2016) 09602.
[5]Q. Barbedienne *et al*., Phys. Rev. B **98** (2018) 195445.
[6] H. Omi *et al*., Phys. Rev. Lett. **72** (1994) 2596.